JOURNAL OF SOLID STATE CHEMISTRY 88, 28–44 (1990)

Analysis of Photoemission Data for CuO: Revision of the Configuration-Energy Scheme for Cuprate Materials

B. H. BRANDOW

Theoretical Division, Los Alamos National Laboratory, Los Alamos, New Mexico 87545

Received April 2, 1990

DEDICATED TO J. M. HONIG ON THE OCCASION OF HIS 65TH BIRTHDAY

The valence-band photoemission and BIS data for CuO, from Sawatzky and co-workers, is reanalyzed using a refined version of their impurity-model treatment. The $2p$-removal spectrum is carefully calculated, as well as the $3d$-removal spectrum. Because a tight-binding treatment of the $2p$ states provides sharp spectral features, and because much of this $2p$ spectrum is unaffected by hybridization with the copper $3d$'s, this provides a distinct marker which serves to clearly determine the charge-transfer energy parameter Δ. We find that $\Delta \gtrsim U$, in contrast to previous studies of cuprates and related transition-metal compounds. The final-state configuration energy ordering is therefore $E(d^8) \lesssim E(d^9\underline{L}) \ll E(d^{10}\underline{L}^2)$. The well-known claim that the doping-induced holes in cuprate superconductors ($La_{2-x}\underline{Sr}_x\underline{CuO}_4$, for example) are hosted almost entirely within $2p$ orbitals is thus disproved. The various kinds of opposing evidence are examined, and reasons for discounting their validity are presented.

Introduction

In studies of the cuprate high-temperature superconductors, it is frequently claimed and widely believed that the holes resulting from doping (e.g., by Sr in $La_{2-x}Sr_xCuO_4$) are accommodated almost entirely within oxygen $2p$ orbitals. This issue is important because these doping holes become the charge-carrying states of the superconductors. We shall present evidence here that this conclusion is wrong, and that the $3d$ character ($3d$ probability) of these holes is quite comparable to their $2p$ character. The analysis provides a new and significantly different set of Anderson impurity model parameters for CuO, which presumably should be close to the parameter values appropriate for Anderson lattice models of the superconducting cuprates. We focus on CuO because this material avoids many complications of the actual cuprate superconductors, including the effects of chain copper and oxygen ions, and the presence of other elements (La, Y, Sr, Bi, etc.). Like pure La_2CuO_4, this material is a magnetic insulator. Also, as in the superconducting cuprates, each copper ion is in square-planar coordination with four nearby oxygens.

At least six types of evidence have been presented for a predominantly $2p$ character of the doping holes: (a) Several spectroscopies (X-ray absorption, core-level photoemission, and electron energy loss) have de-

0022-4596/90 $3.00

tected holes in $2p$ orbitals, especially in samples with enough hole-doping to exhibit superconductivity (*1*). (b) Searches for $3d^8$ configurations (or for "Cu^{3+} ions") with the same spectroscopies have typically failed to find evidence for these (*1*). (c) Analyses of valence-band photoemission and inverse photoemission (bremsstrahlung isochromat spectroscopy, or BIS) data have generally placed the final-state $3d^8$ configuration energy far above the $3d^9\underline{L}$ and $3d^{10}\underline{L}^2$ energies, by at least several electron volts (*2–4*). [$\underline{L}$ denotes a "ligand" or oxygen $2p$ hole.] (d) At the copper $3p \rightarrow 3d$ resonance (incident photon energy near 74 eV), some of the states in the "satellite" part of the photoemission spectrum (6–11 eV above the main peak for CuO) are strongly enhanced. Because the mechanism for this resonance specifically involves $3d^8$ final states, this is claimed (*3, 4*) as direct evidence that $E(3d^8)$ lies well above $E(3d^9\underline{L})$ and/or $E(3d^{10}\underline{L}^2)$. (e) The quantitative energy-level ordering found for cuprates is quite reasonably related to the corresponding energy orderings derived from (c) and (d) for a number of other transition-metal compounds (*5–7*), including the copper dihalides ($CuCl_2$, etc.), and the prototype Mott insulator NiO. (f) Analyses of local-density band calculations have provided small Δ values (*8, 9*). Our disagreement with the prevailing picture thus has implications beyond the field of high-temperature superconductivity.

We accept point (a) at face value; it is entirely reasonable that the doping holes should be *partially* accommodated in oxygen $2p$ orbitals. We note, however, that the evidence (b) for $3d^8$ configurations is *not* uniformly negative (*10*). Problems here include the possibility of oxygen loss from the superconductor samples, chemical instability of the Cu^{3+} reference compounds, and the need for very detailed theoretical analysis of the X-ray and electron energy loss absorption edges. (It is worth noting, here, that the photoemission problem of surface oxygen loss has recently been shown to be more severe than previously recognized (*11*).) The evidence (f) from local-density band theory is also unreliable, in view of the well-known failure of this approximation to explain the Mott features (insulation and antiferromagnetism) of undoped La_2CuO_4.

In this paper we reexamine the evidence (c) from photoemission and BIS for CuO, and argue that this data has been wrongly interpreted. This criticism may well apply also to other compounds in point (e) above, thus the argument from general systematics is also suspect. (We have argued previously (*12*) that the prevailing interpretation is in conflict with the photoemission systematics of other transition-metal oxides (*13, 14*).) On the other hand, the evidence (d) from resonant photoemission appears quite strong, especially in view of a recent study providing a detailed theoretical fit (*15*). (See also Ref. (*16*) for NiO.) This evidence cannot be dismissed lightly. However, we shall argue here that a conspicuous feature of the ordinary (nonresonant) photoemission data now opens a way to reconcile the resonance data with our present results. We have therefore concluded, from all of these considerations, that a careful analysis of photoemission and BIS data should take precedence over the other evidence cited above.

Data Analysis

We use the recent CuO photoemission and BIS data of Sawatzky and co-workers (*3, 4*), which is reproduced here in Fig. 1. Our method of analysis is basically the same as that of Eskes, Tjeng, and Sawatzky (ETS) (*4*), the most refined analysis to date, but there are significant differences of detail. We shall focus on the differences, and refer the reader to ETS for further description and background material. We use an Anderson impurity model, in contrast to their CuO_4 cluster model, thus we are treating the oxygen $2p$ orbitals as band states. (As in ETS,

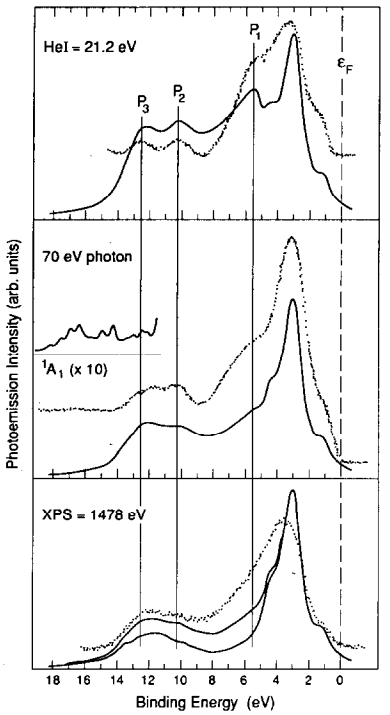

FIG. 1. Experimental photoemission intensities for CuO at three photon energies, from ETS (Ref. (*4*)), and the corresponding theoretical results (solid lines). The latter all incorporate Lorentzian broadening with half-width of 0.6 eV. The lowest curve is the pure d-removal intensity. The insert shows the theoretical result for the weak $^1A_1$ d-removal intensity at high binding energy, calculated with a reduced Lorentzian half-width of 0.2 eV and magnified by a factor of 10. The $E = 0$ reference energy, labeled ε_F, may not accurately represent the true Fermi energy for CuO.

the model also includes Coulomb and exchange interactions among the copper $3d$ orbitals, and hybridization between the copper $3d$'s and oxygen $2p$'s, but it ignores Coulomb interactions involving the $2p$'s.) The single copper ion (the "impurity") has square-planar coordination with four neighboring oxygens, and therefore the orbitals and the multielectron (hole) states are classified according to the D_{4h} point group. For example, the $3d$ orbital types become $b_{1g} = x^2 - y^2$, $a_{1g} = 3z^2 - r^2$, $b_{2g} = xy$, and $e_g = (xz, yz)$. The full two-hole multiplet structure for D_{4h} is calculated, as in ETS, using the appropriate Coulomb (and exchange) matrix elements (*4, 7*), which are expressed in terms of the Racah A,B,C parameters. The main distinguishing feature of our analysis is a very detailed treatment of the oxygen $2p$ states, and we now present the motivation for this.

Because the atomic-orbital photoemission cross sections (σ_{2p}, σ_{3d}) have quite different dependences on the kinetic energy of the final-state photoemitted electron, (*14, 17*), the XPS (1478 eV photon) data in Fig. 1 is mainly due to $3d$ photoemission, while the HeI (21.2 eV photon) spectrum has a strong contribution from $2p$ photoemission. By comparing these two spectra, we conclude that the $2p$-emission intensity has *three prominent features,* labeled P_1–P_3 in Fig. 1. The 70-eV photon data has good resolution and also clearly shows these features. However, the HeII (40.8 eV) data (*3, 15*) do not closely resemble a simple interpolation between the HeI and 70-eV data, and the reason for this is unclear. We have therefore largely ignored this HeII data.

In seeking to understand features P_1–P_3, we first examine the square cluster of four oxygens surrounding the "impurity" copper ion. This cluster has 12 spatial orbitals of $2p$ character. After rearranging these orbitals into symmetry-adapted combinations ϕ_γ for the D_{4h} point group, we observe that more than half of the latter orbitals (7 out of 12) have symmetries which forbid them from hybridizing with any of the $3d$ orbitals. This suggests that a simple tight-binding band calculation for the $2p$'s might go far towards explaining features P_1–P_3.

The monoclinic crystal structure of CuO can be viewed as a distortion of the tetragonal PdO structure, in which the oxygen ions form a simple cubic lattice (ignoring some c-axis contraction) (*18*). We therefore assume a simple cubic lattice for the oxygens. Keeping only nearest-neighbor transfer in-

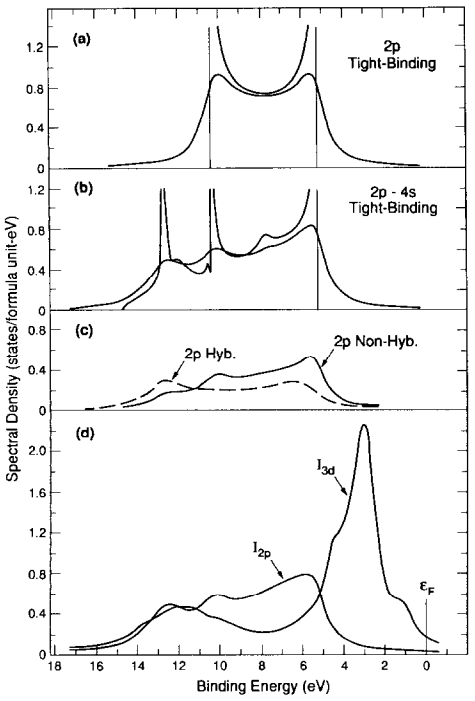

FIG. 2. (a) $2p$ state density; tight-binding calculation for simple-cubic oxygen lattice. (b) $2p$–$4s$ state density; tight-binding calculation for idealized PdO lattice with $4s$ orbitals on the Pd sites. (c) Total $2p$ projected state density for the nonhybridizing orbital symmetries, and total $2p$-removal intensity for the hybridizing symmetries (with hybridization). (d) Total $2p$- and $3d$-removal intensities. The intensities are expressed as effective state densities. All smooth curves incorporate Lorentzian broadening with half-width of 0.6 eV.

tegrals, the p electron tight-binding problem becomes quite elementary; this separates into three equivalent one-dimensional chain problems, for the p_x, p_y, and p_z orbitals, respectively. Each of these chains has a simple cosine dispersion, producing the form of state density shown in Fig. 2a. We associate the resulting two prominent singularities with the experimental features P_1 and P_2. To account for P_3, we recall that band-structure calculations for NiO and La_2CuO_4 have revealed a strong influence due to the $4s$ orbitals of the transition-metal ions (*8, 19*). (The $4s$ and the $2p$ orbitals are both quite extended, and therefore have a large spatial overlap.) We therefore return to the idealized PdO structure (with simple cubic oxygen lattice), place a $4s$ orbital on each Pd lattice site, and repeat the tight-binding calculation with a Slater–Koster parameter (*20*) $(sp\sigma)$ coupling each $4s$ to its nearest-neighbor $2p$'s, where allowed by symmetry. This produces the total $2p$–$4s$ state density shown in Fig. 2b (with the higher-energy "$4s$" region omitted). The $4s$'s are seen to interact with some, but not all, of the states near the bottom of the pure $2p$ band of Fig. 2a, pushing these states further down and producing a third peak. The top of the $2p$ band remains unaffected, however, and it therefore ends up providing the most intense feature. Good correspondence with P_1–P_3 is obtained by using the (hole) parameter values $\varepsilon_{2p} - \varepsilon_{4s} = 10$ eV, $t_{pp} = (pp\sigma) = 1.3$ eV, $t_{sp} = (sp\sigma)/\sqrt{2} = 2.1$ eV; these values are reasonably consistent with band theory (*8, 21*). (This t_{pp} is twice the value often quoted, because our $2p$ basis functions are directed toward the neighboring oxygen ions, instead of towards the copper ion.)

This tight-binding calculation needs some further refinement, for use within the Anderson impurity model. We return to the simple four-oxygen cluster, and examine each of its 12 spatially distinct symmetry-adapted $2p$ orbitals ϕ_γ. For each one of the latter, we calculate its overlap with the tight-binding Bloch eigenstates $\psi_{k\nu}$ (ν is a band index), and thus determine its projected state density

$$\rho_\gamma(\varepsilon) = \sum_{k\nu} |\langle \phi_\gamma | \psi_{k\nu} \rangle|^2 \delta(\varepsilon - \varepsilon_{k\nu}). \quad (1)$$

For the symmetries $\gamma = b_{1g}$, a_{1g}, b_{2g}, e_g, which can hybridize with d orbitals, the corresponding hybridization weight distributions (*22*) are then $T_\gamma^2 \rho_\gamma(\varepsilon)$, where T_γ is the $2p$–$3d$ transfer integral for ϕ_γ and its $3d$ partner orbital. (These distributions have been calculated previously (*22*) for La_2CuO_4 using, however, the conventional band structure.) We model each of these hybridization

weight distributions by discretizing into 10 states (*23*). Each hole in one of these symmetries is thus represented by 11 states, 10 for the $2p$ band states plus 1 for the $3d$ component. At this stage, the two-hole eigenstates (those reached by photoemission) are computed by matrix diagonalization. The spectral weights for $2p$ removal and for $3d$ removal are then constructed according to the sudden approximation (equivalent to the usual Greens function expression), and these results are then broadened by a Lorentzian with Γ (*hwhm*) = 0.6 eV, for the sake of illustration. To this $2p$ spectral weight (from the hybridizing γ's) we then add the sum of all of the remaining ($3d$-nonhybridizing) projected $2p$ state densities (Eq. (1)), similarly broadened, to obtain the *total* spectral density for $2p$ removal. These spectral densities are shown in Figs. 2c and 2d. (The $2p$ spectral densities have been divided by 4, to normalize to one oxygen ion per copper ion. For ease of comparison, all intensities have been expressed as effective state densities, and similarly in Fig. 4 below.) It is clear here that the $2p$ spectral features P_1–P_3 are largely determined by the nonhybridizing part of the $2p$ density. In fact, these features have almost the same form as if they came directly from the total tight-binding state density of Fig. 2b.

The use of the projected state densities $\rho_\gamma(\varepsilon)$ introduces an effective crystal-field splitting for the symmetry-adapted $2p$ orbitals ϕ_γ. The centroids of these state-density distributions may be regarded as the energies $\varepsilon_p(\gamma)$ of the ϕ_γ orbitals in the associated CuO_4 cluster model. The resulting (hole) splittings for the hybridizing symmetries are

$$\begin{aligned} \varepsilon_p(e_g) - \varepsilon_p(b_{1g}) &= 1.8\,\text{eV} \\ \varepsilon_p(b_{2g}) - \varepsilon_p(e_g) &= 1.8\,\text{eV} \\ \varepsilon_p(a_{1g}) - \varepsilon_p(b_{2g}) &= 1.5\,\text{eV}. \end{aligned} \qquad (2)$$

The corresponding ETS model values are 1.0 eV, 1.0 eV, and zero, for these energy differences. (These ETS splittings came from a single parameter, fitted to the photoemission data.) In an earlier work, Eskes and Sawatzky (*4*) employed an impurity model with a simple (semielliptic) $2p$ band density, but without any symmetry projection, thereby omitting entirely this $2p$ splitting. The $\rho_\gamma(\varepsilon)$'s for the four hybridizing symmetries are shown in Fig. 3, with their centroids marked. It is clear that a part of the large (1.8 eV) separations is due to the influence of the $4s$ orbitals, and that all of the a_{1g}–b_{2g} separation is due to these orbitals.

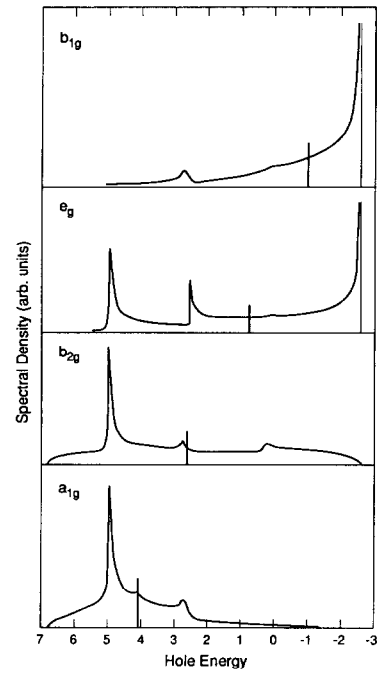

FIG. 3. Projected $2p$ state densities $\rho_\gamma(\varepsilon)$ for the four hybridizing symmetries γ, with their centroids marked by vertical lines. The origin of the energy scale is the $2p$ energy input ε_p for the tight-binding calculation.

Other differences from the analysis of ETS are the following: (1) The charge-transfer parameter Δ [nominally $E(d^{10}\underline{L})$-$E(d^9)$, see Refs. (*5*, *6*)] is defined here according to the one-hole ground state calculation, namely, as the difference between the centroid of the $2p$ hole state density of b_{1g}

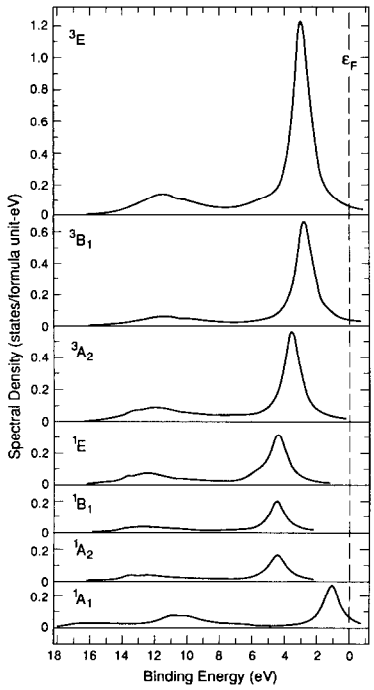

FIG. 4. The individual d-removal spectra for the seven hybridizing two-hole channels (irreducible representations of D_{4h}) which contribute to the total d-removal spectrum. Each spectrum includes the appropriate statistical weight, and is broadened by a Lorentzian with half-width of 0.6 eV. The intensities are expressed as effective state densities.

symmetry, $\rho_{b1g}(\varepsilon)$, and the $3d$ hole energy for this symmetry. (The recipe of ETS corresponds to using the center of a simplified $2p$ band, or the center of a $2p$ cluster spectrum.) Our definition makes Δ significantly smaller than it would be with the ETS definition [see Eq. (2) and Fig. 3], thus the fact that we obtain a much larger Δ is not at all due to this different definition. (2) We extract an experimental quantity U_{Mott} = E(BIST) + E(PET), where the latter are the BIS and photoemission threshold energies, expressed as absolute differences from the Fermi energy. In each case we take the *peak position* of the leading experimental feature, as appropriate for localized excitations. This is more straightforward and reliable than the procedure of ETS, who tried to compare the actual thresholds, thus requiring estimates of the intrinsic broadenings in both theory and experiment. We thereby obtain E(BIST) = 1.8 eV and E(PET) = 1.1 eV, so that our model should reproduce U_{Mott} = 2.9 eV. This is much larger than the corresponding quantity of ETS, their E_{gap} = 1.8 eV. (This discrepancy is also related to the interpretation of E_{gap}; see Discussion.) (3) ETS have assumed that $T_{b2g} = \frac{1}{2} T_{b1g}$. We have relaxed this assumption, although we retain their assumptions $T_{a1g} = T_{b1g}/\sqrt{3}$ and $T_{eg} = T_{b2g}/\sqrt{2}$, since the latter ratios follow from the Slater–Koster parametrization (*20*) of the transfer integrals. (Nevertheless, a modification for T_{a1g} is described below.) The differences among these T_γs are responsible for much, but certainly not all, of the phenomenological crystal-field splitting. (4) Our "bare" $3d$ energy levels are split apart by an assumed *nonhybridization* component of the crystal field, as has been found in previous ab initio studies of $3d$ ion clusters (*24*). These studies indicate that this component arises mainly from the increase of kinetic energy due to mutually orthogonalizing the $3d$ and $2p$ orbitals, i.e., due to replacing atomic orbitals by Wannier orbitals. We parametrize this effect by assuming $3d$ energy shifts (for electrons, not holes) proportional to the squares of the $2p$–$3d$ transfer integrals T_γ, thus

$$\delta\varepsilon_d(\gamma) = (T_\gamma/T_{b1g})^2\Delta_{CF}^{\circ}. \qquad (3)$$

[Our Δ parameter is the separation between the b_{1g} $2p$ hole centroid and the *final*, Δ_{CF}°-shifted, value of the hole $\varepsilon_d(b_{1g})$.] (5) Our Racah B and C parameters are obtained by linear extrapolation from the $3d$ transition metal values of Tanabe and Sugano (*25*), for 3+ ions, which gives B = 0.145 eV, C = 0.715 eV. (This procedure avoids the screening effect of a $4s$ electron, in the free-ion $3d^8 4s$ states which apparently were ana-

lyzed by ETS.) The effects of thus revising B and C are quite minor. Two further refinements are described below, in connection with Eqs. (4) and (5).

Having fixed B,C, and the $2p$ tight-binding parameters as described above, there remain five adjustable parameters to describe the $3d$ electrons: Δ, A, Δ_{CF}°, T_{b1g}, and T_{b2g}. Our criteria for fitting these parameters are the following: Δ is determined to place the strongest $2p$ feature, P_1, the correct distance from the main peak. (The latter, 3.0 eV from ε_F, is mainly due to a very intense ^3E state in the d-removal spectrum.) The Racah A is chosen to reproduce U_{Mott}. Δ_{CF}° is chosen to obtain the observed separation (1.9 eV) between the main peak and the first ionization state [a $^1A_1$ state of modest intensity, at $E(\text{PET}) = 1.1$ eV from ε_F].

The criteria for T_{b1g} and T_{b2g} are less direct. Well beyond the satellite region, and 13.6 eV beyond the main peak, a very faint peak can be seen in the 70 eV data of Fig. 1. We indeed find some weak intensity in this region, composed of $^1A_1$-state contributions to the d-removal intensity, in agreement with ETS. However, this feature is masked in the theoretical spectra by the Lorentzian tails from our assumed broadening function. This part of the $^1A_1$ intensity is shown in an insert in Fig. 1, magnified by a factor of 10 and now resolved by decreasing the Lorentzian half-width to 0.2 eV. [Some of the fine structure here may be an artifact of our discretization of the ρ_γ distributions.] T_{b1g} and T_{b2g} are determined by the position, shape, and intensity of this high-energy $^1A_1$ structure, together with these features of the XPS satellite. [Alternatively, we could have fixed T_{b1g} by the value of E(BIST), but we rejected this because the true ε_F for CuO is quite uncertain. The quoted ε_F is merely a convenient reference energy, the Fermi level of a clean copper electrode. It should be noted that this uncertainty does not affect U_{Mott}.]

In order to obtain sufficient intensity for the high-energy $^1A_1$ feature, and likewise for the XPS satellite (i.e., the d-removal intensity between 8 and 14 eV), we found it necessary to employ a further refinement. We use different values for the T_γs which produce the d^8–d^9 and d^9–d^{10} transitions; these are denoted as $T_{\gamma 8}$ and $T_{\gamma 10}$, respectively (*15*). This introduces just one more independent parameter [T_{b1g8} and T_{b1g10}, vs the previous T_{b1g}], since the other Ts are assumed here to scale as

$$T_{\gamma 10} = T_{\gamma 8} T_{b1g10} / T_{b1g8}. \tag{4}$$

This modification is quite reasonable on ab initio grounds (see Discussion), and in fact our ratio T_{b1g10}/T_{b1g8} is close to that found in a quantum-chemical cluster calculation (*26*). This feature of charge-dependent Ts has been found previously in other phenomenological studies (*15*).

There is still a significant defect in the model described so far. With reasonable parameters, this model places a fairly intense $^3B_1$ state about midway between the main peak and the $^1A_1$ threshold state. Experimentally, however, this $^3B_1$ state seems to be merged with the strong ^3E state, thus contributing to the great intensity of the main peak, and at the same time allowing the weak $^1A_1$ threshold state to be resolved. (The position of this $^3B_1$ state is not a problem in the work of ETS, but it becomes so when some of our refinements are included.) It is mainly the effective splitting between the e_g and a_{1g} antibonding (d-like) molecular orbitals which determines the ^3E–$^3B_1$ separation, so this indicates that there is some deficiency in our treatment of the crystal-field splitting. It is known, however, that an unexpected shift of the a_{1g} antibonding state, of the desired sign and general magnitude, is typical in spectroscopic studies of square-planar complexes, including those of Pd, Pt, and Au, as well as Cu. Molecular-orbital calculations (*27*) have shown that this is due to strong participation of a metal s

TABLE I

ANDERSON IMPURITY MODEL PARAMETERS (IN eV)

	Present results	ETS
Δ	7.55	2.75 1.75*
A	4.3	6.5
$U_{\text{eff}}(^1A_1)$	7.0	8.8
T_{b1g8}	3.8	2.5
T_{b1g10}	2.9	
T_{b2g}	1.5	1.25
Δ_{CF}°	2.05	0
f_{a1g}	0.25	1.0

*Present definition, see text.

orbital (here the copper 4*s*), which is possible only for the a_{1g} symmetry.

The energies of the a_{1g} antibonding molecular orbitals are determined in our model by the parameters $\varepsilon_d(a_{1g})$, T_{a1g8} [and T_{a1g10} from Eq. (4)], and $\rho_{a1g}(\varepsilon)$. The ρ_{a1g} distribution already includes a strong influence from 4*s* orbitals, and it is questionable whether we should modify $\varepsilon_d(a_{1g})$, since the same-site 3*d* and 4*s* orbitals do not interact directly. This suggests that we should focus on the $T_{a1g\nu}$'s (ν = 8,10). We have therefore added another parameter f_{a1g} to reduce the magnitudes of the $T_{a1g\nu}$'s,

$$T_{a1g\nu} = (f_{a1g}/3)^{1/2} T_{b1g\nu}, \tag{5}$$

viewing this as merely an artifice to mimic an effect of the 4*s* orbitals. These $T_{a1g\nu}$'s have been used throughout the present model, including Eq. (3) to determine $\delta\varepsilon_d$ (a_{1g}), so that we are compromising on the issue of modifying ε_d (a_{1g}). f_{a1g} was determined to make the a_{1g} and e_g crystal-field excitation energies coincide, within the context of the optical absorption states of the 2+ copper ion. This arbitrary but reasonable recipe places the $^3B_1$ peak about 0.15 eV to the right of the ^3E peak, too close to the latter to be resolved.

Table I shows the parameters of our best fit, determined as described above. This also shows the corresponding results of ETS, who assumed that $T_{b2g} = \frac{1}{2} T_{b1g}$. For comparison, the band-theoretic results of McMahan *et al.*, (*8*), for La_2CuO_4, give T_{b1g} = 3.2 eV and T_{b2g} = 1.5 eV. Some important features of these results will be discussed below. The individual spectra for the seven different two-hole channels (irreducible representations of D_{4h}) which contribute to the total *d*-removal spectrum are shown in Fig. 4, broadened again by a Lorentzian with half-width of 0.6 eV. Each of these spectra includes the appropriate statistical weight (*4*).

As the final step of this analysis, we have combined the present 2*p*- and 3*d*-removal spectra with adjustable relative weights, in order to compare with the HeI, 70-eV photon, and XPS data in Fig. 1. The results are shown as solid lines in Fig. 1, where we have used σ_{2p}/σ_{3d} = 1.6, 0.6, and 0.4, respectively, for the photoemission cross section ratios. The corresponding theoretical ratios are 3.6, 0.7, and 0.04, calculated from neutral-atom orbitals (*17*). (Each of the present σs refers to a *single* atomic orbital, averaged over the subshell.) The *energies* of essentially all of the experimental features are reproduced well. However, there are a number of problems for the *relative intensities*. We shall now try to construct a consistent picture to resolve these problems, admittedly at the cost of much rationalization.

It is simplest to compare with the XPS data, because the momentum of the photoemitted electron is so large here that, after averaging over grain orientations in the sample, the interference between emission amplitudes from different sites is safely negligible. The shape and intensity of the satellite are reproduced quite well. Nevertheless, it seems surprising that the required σ_{2p}/σ_{3d} ratio is so large (0.4 vs 0.04). The main explanation is probably that removal of a 3*d* electron drastically

alters the local Coulomb potential, which leads to extensive orbital rearrangement (orbital relaxation) for the "passive" electrons. The relevant processes here are contractions of the $3d$ orbitals, distortions of the $2p$ orbitals, and a backflow or screening charge transfer involving oxygen $2p$, $2s$ to copper $3d$, $4s$, $4p$ virtual transitions (except, of course, for the $2p \rightarrow 3d$ charge transfer which is treated explicitly here). The result is to reduce the overlap between the initial- and final-state wavefunctions, which thereby reduces the d-removal intensity. A simple argument (*28*) shows that the intensity reduction factor should be of order $e^{-1} = 0.37$, and even stronger reduction (say, 0.2) would not be unreasonable. [The sum rule for the total d-removal intensity should be satisfied by higher-energy contributions, corresponding to shake-ups such as $3d \rightarrow 4d$ and $2p \rightarrow 4s$.] The $2p$ orbitals are much more diffuse, so the corresponding reduction of the p-removal intensity should be a far weaker effect. The net result is an apparent strong enhancement of the p-removal intensity.

Another contribution to the apparent large $2p$ intensity should arise from the fact that the theoretical analysis presumes the use of orthogonal orbitals, i.e., Wannier functions, which must be constructed out of atomic (or ionic) orbitals. Thus, when a photon is absorbed by a $3d$ atomic orbital, a possible result can be photoemission from a $2p$ Wannier orbital. This $3d \rightarrow 2p$ contribution is weak, amounting to only a few percent of the direct $2p$ intensity. [In fact, in the satellite region this tends to have a negative effect on the intensity, due to destructive interference between the direct ($3d$) and indirect ($3d \rightarrow 2p$) amplitudes.] However, the $2p$ Wannier orbitals also receive a number of similar contributions from the copper core orbitals, and at the XPS energy the latter all have larger photoemission cross sections than the $3d$ orbitals. The combined effect of all of this "orthogonality mixing" may therefore be significant. There is some evidence for this in that the P_1 feature appears to be contributing substantially to the XPS spectrum, considerably more so than in our theoretical XPS spectrum, even though the P_1 feature is not directly discernable due to the poor XPS resolution. The P_1 feature is due mainly to the b_{1g} channel, ρ_{b1g} from Eq. (1) (see Fig. 3), for which the orthogonality mixing contributions should be strongest.

Turning to the 70-eV data, we find σ_{2p}/σ_{3d} to be roughly 0.6, from the satellite shape. However, it is quite obvious that in the satellite region both the d- and p-removal intensities are now very much weakened (by factors of around 1/4) with respect to the theoretical spectra. This feature is even more pronounced in the HeI data, and in the recent CuO resonance study (*15*) this is seen to be a systematic trend. Furthermore, the latter data show that the high-binding-energy shoulder of the satellite is generally suppressed more than the low-energy shoulder. (This appears to indicate suppression of the hybridizing $2p$ contribution, see Fig. 2c.) Crudely speaking, it appears that the theoretical spectrum is being suppressed by a continuously decaying function of the binding energy, say $\exp[-\lambda \cdot \mathrm{BE}]$, with λ, the strength of this effect, increasing monotonically with decreasing photon energy. We attribute this to a progressive breakdown of the sudden approximation, i.e., a tendency toward adiabatic behavior (*29*), whereby part of the satellite intensity is transferred to the main peak. Unfortunately, this feature obscures the interpretation of the empirical σ_{2p}/σ_{3d} value, since one would expect this effect to be stronger for d-electron removal.

Subject to this caveat, the P_1 feature again seems to be relatively enhanced, in the 70-eV data, consistent with the orthogonality-mixing mechanism. Also, the "middle

peak" in the satellite (at 11.6 eV) appears more prominent than in the theoretical spectrum. The above-mentioned stronger adiabatic suppression of the left-hand side of the satellite might account for this.

For the HeI data, our cross-section ratio of 1.6 refers to the P_1 vs main peak relative intensity. This is still significantly less than the atomic-orbital prediction of 3.6, but at such low photon energy one may expect some significant interference between emission from orbitals on different sites, including $2p$–$3d$ interference. There should also be some main-peak d enhancement due to adiabaticity. Adiabatic suppression of both p and d intensity in the satellite region is now quite extreme, to the point where the d contribution is now invisible. Because σ_{2p}/σ_{3d} is now so large, the effect of orthogonality mixing within the Wannier $2p$'s should be less significant here, and P_1 should not be enhanced. There is, however, now a converse effect—intensity enhancement for removal of the Wannier $3d$ with b_{1g} symmetry, due to its atomic $2p$ content—which seems to be increasing the intensity of the threshold $^1A_1$ state.

In judging the goodness of the present theoretical fits, one should allow for the P_1 feature being broadened considerably more, due to the distortion of the oxygen lattice away from the assumed simple-cubic form. The threshold $^1A_1$ state also appears to be more broad than our assumed Lorentzian half-width of 0.6 eV. The great strength of the b_{1g} hybridization should indeed give this state extra width. We should also point out that, for the experimental results in Fig. 1, we have shifted the HeI and XPS main peak positions slightly with respect to the 70-eV data (which has the best resolution), to correct for apparent shifts due to the strong tails of their P_1 features.

It should also be noted that we have envisaged the adiabaticity as entering in two stages. Below some fairly high energy (apparently $\gg$ 70 eV), the d-orbital (and probably the p-orbital) relaxations become adiabatic with respect to the outgoing photoelectron, thus turning off the d-intensity suppression seen in the XPS data. At lower photon energies (and already by 70 eV), the $2p \rightarrow 3d$ charge transfer "backflow" is becoming adiabatic, thus turning off the satellite intensity. Obviously, the entire discussion of adiabaticity here is conjectural, but this appears to be required by the data.

Discussion

There are a number of significant differences between the present phenomenological model and that of ETS (*3*, *4*), the most refined previous study: (1) a tight-binding band treatment of the oxygen $2p$ orbitals, (2) use of the projected $2p$ state densities $\rho_\gamma(\varepsilon)$ for the various local (D_{4h}) symmetries γ, (3) inclusion of some effects of the $4s$ orbitals, (4) a considerably larger input value for the experimental quantity U_{Mott}, (5) allowance for charge dependence in the transfer integrals T_γ, and (6) allowance for a nonhybridization component Δ_{CF}° of the $3d$ crystal field splitting. Each of these refinements has a significant influence on the calculated results, and is therefore important for a realistic determination of the model parameters. Some other refinements have also been included.

The $4s$ orbitals play an important role, especially in altering the effective crystal fields experienced by the p and d orbitals of a_{1g} ($=3z^2 - r^2$) symmetry. The $2p$ hole energy [the $\rho_{a1g}(\varepsilon)$ centroid] is raised about 3 eV due to hybridization with the $4s$ orbitals. The remaining effect of mapping the three-dimensional ($2p$, $3d$, $4s$) hybridization onto an equivalent ($2p$, $3d$) problem is treated here by a reduction of the effective p–d hybridization strength T_{a1g}. The main result is to shift the antibonding (d-like) molecular-orbital a_{1g} level close to the corresponding b_{2g} ($=xy$) and e_g($=$ xz, yz) levels, so that

these are *all* widely separated from the b_{1g} ($= x^2 - y^2$) level. This feature now provides a strong justification for focusing on only the $3d$ orbitals of b_{1g} symmetry, in model-Hamiltonian studies of pairing mechanisms for cuprate superconductivity.

Because our present $\Delta \gtrsim U$ type of solution cannot be obtained without inclusion of the Δ_{CF}° parameter, it is important to emphasize that the physical effect (orthogonality repulsion) which we have parameterized by Δ_{CF}° is genuine (*24*). The magnitude found for Δ_{CF}° might seem unreasonably large, however, until one recalls that the empirical crystal-field splittings of 3+ ions are generally much larger (by as much as a factor of two) than for their 2+ counterparts, for the $3d$ transition metals (*30*). Furthermore, the feature of square-planar coordination (rather than octahedral) reduces the Cu–O bond length (1.95 Å) significantly below the value (2.06 Å) which one can extrapolate from the preceding transition metal monoxides, and this should increase both the hybridization and nonhybridization (Δ_{CF}°) components of the crystal field. This latter consideration seems inadequate, however, to explain the large magnitude of the present Δ_{CF}°. We interpret this as evidence that the $2p$ orbitals of the neighboring O^{2-} ions, which are quite diffuse and bound only by the Madelung potential, are pulled in closer to the copper 3+ ion, creating a stronger orthogonality–repulsion effect than for the case of the 2+ ion. (This more than compensates for the contraction of the $3d$ orbitals in the 3+ state.) This picture is supported also by the larger magnitude found for T_{b1g8}, as compared to T_{b1g10}. Thus, although the present Δ_{CF}° is almost certainly too large to properly describe the $d \rightarrow d^*$ optical absorptions within the Cu^{2+} ground state configuration (absorptions which are dipole forbidden and therefore presumably weak), we argue that this large Δ_{CF}° is not excessive for the photoemission final states.

The magnitudes of Δ and U_{eff}, the effective Hubbard U, are of particular interest. As emphasized by ETS, this U_{eff} is quite state dependent. We shall focus on the states of $^1A_1$ symmetry, which include the first ionization state. These states arise from two holes of b_{1g} symmetry, so this choice is appropriate for simplified Anderson models which effectively contain only the $3d$ orbitals of this symmetry, as in Ref. (*12*). The appropriate U is then the Coulomb interaction between two of these $3d$ orbitals (*4, 7*),

$$U_{\text{eff}}(^1A_1) = A + 4B + 3B, \qquad (6)$$

which is 7.0 eV here. This is close to our $\Delta = 7.55$ eV. The results of ETS are very different: $A = 6.5$ eV, $U_{\text{eff}} = 8.8$ eV, and $\Delta = 2.75$ eV (their definition) or 1.75 eV (our definition). We now recall that (*5, 6*)

$$E(d^{10}\underline{L}^2) - E(d^9\underline{L}) = \Delta \qquad (7)$$

$$E(d^9\underline{L}) - E(d^8) = \Delta - U_{\text{eff}},$$

for the configuration energies of the corresponding CuO_4 cluster model. [The $\underline{L}$ energy corresponds to the centroid of the b_{1g} projected state density, Eq. (1) and Fig. 3, for $2p$ hole states.] The large differences in the magnitudes of Δ and $\Delta - U_{\text{eff}}$ therefore correspond to strikingly different relative-energy schemes, as shown in Fig. 5. Note

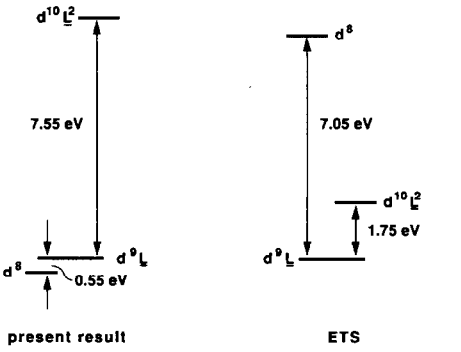

FIG. 5. The cluster configuration energy scheme of the present analysis, and that of ETS (Ref. (*4*)), for the $^1A_1$ states of two holes of b_{1g} symmetry.

especially that $\Delta - U_{\text{eff}}$ has changed by 7.6 eV. The large change in Δ is required, here, in order to place the $2p$ features, P_1–P_3, in their correct positions with respect to the main peak. This $2p$ evidence has not been considered previously in studies of cuprate materials, or in much of the work on related transition-metal compounds.

In the ETS scheme, where $d^9\underline{L}$ and $d^{10}\underline{L}^2$ both lie considerably below d^8, a doping hole would obviously have almost pure $2p$ character. In contrast, we now find the lowest configurations to be d^8 and $d^9\underline{L}$. Because the latter are separated by much less than their effective mixing matrix element, $\sqrt{2}\,T_{b1g8}$, a doping hole should have quite comparable amounts of $3d$ and $2p$ character. This has indeed been confirmed experimentally, in recent studies of photoemission near ε_F in metallic cuprates (*11*). This strong p–d mixing for the doping holes is also supported by ab initio quantum-chemistry cluster calculations with accurate nonlocal exchange (*26*).

For a simple qualitative understanding of the present theoretical spectra, one can visualize the main peak and the satellite as coming from the bonding and antibonding combinations of d^8 and $d^9\underline{L}$. (This applies to each of the channels in Fig. 4. The $d^{10}\underline{L}^2$ configuration typically plays only a minor role, except for high-lying states with negligible intensity. Since the $2p$ band states are largely nonbonding, most of the $2p$ removal intensity is found in between the main peak and the satellite.

The present configuration-energy scheme, $E(d^8) \lesssim E(d^9\underline{L}) \lesssim E(d^{10}\underline{L}^2)$, was anticipated by a variety of arguments in Ref. (*12*). In particular, we noted there that reliance on the $3d$ spectrum alone leads to an ambiguity: The d^8 and $d^{10}\underline{L}^2$ configuration energies can be interchanged, with little effect on the spectrum. (Due to a symmetry of the energy matrix, this interchange would have *no effect* on the final-state eigenvalues, for a cluster model with crystal-field multiplet structure ignored,as in the treatment of Shen *et al.* (*2*).) This point is confirmed in Fig. 5, which shows that the d^8 and $d^{10}\underline{L}^2$ energies have indeed been roughly interchanged. We also observed that the photoemission systematics of other transition-metal oxides (*13, 14*) strongly supports the present configuration-energy scheme. The latter evidence is of two kinds: (a) a near-constancy of the energy separation between the oxygen $2s$ and $2p$ features (for the materials where the latter can be identified), and (b) a $3d$-like photon energy dependence for the relative intensity of the "main peak" (near photoemission threshold), which also exhibits the d^{n-1} multiplet structure expected from crystal-field theory, and a $2p$-like dependence for intensity somewhat above this main peak. The CuO data shares all of these characteristics, if we take P_1 to be "the" $2p$ feature.

In connection with point (a), concerning $2p$ features which were seen at X-ray (>1000 eV) photon energies (*13*), we note that the present XPS data analysis revealed unexpectedly strong $2p$ contributions. We attributed this $2p$ strength to a relative suppression of the d intensity, and to an enhancement of the feature (P_1) at the top of the $2p$ band, due to the much greater strength of orthogonality mixing in the b_{1g} channel. It now appears that these features may be rather general, i.e., insensitive to details of the local oxygen coordination geometry, so that they may be generic for transition-metal oxides.

We now describe two further kinds of evidence for the present configuration-energy scheme, evidence which has helped to motivate this investigation. First, in ionic compounds of $3d$ transition metals, 3+ ions typically have much larger phenomenological crystal-field splittings than the corresponding 2+ ions (by roughly a factor of two) (*30*): $\Delta_{CF}^{3+} \gg \Delta_{CF}^{2+}$. Since a significant part of these Δ_{CF}s should come from the $2p$–$3d$ hybridization, and since the hybridization contribution to the relevant antibonding state

energies depends on the separation between the unhybridized configuration energies, this strongly suggests that (*31, 32*)

$$|\Delta| \gg |\Delta - U_{\text{eff}}|. \tag{8}$$

The present results satisfy this criterion, while the conventional results (*2–7*) do not. Our finding of stronger hybridization in the 3+ state, $|T_{\gamma 8}| > |T_{\gamma 10}|$, tends to weaken this argument,as does also our expectation of a similar charge dependence for Δ_{CF}°, but we doubt that these considerations can suffice to justify the conventional picture.

The second kind of evidence comes from the optical-absorption spectra of NiO, CoO, and MnO. Their strong-absorption "edges" (located at $\lesssim 4$ eV) are not very abrupt, and in fact display considerable structure, over a range of several electron volts. Furthermore, these structures differ significantly among these compounds. It has long been known that the differences among these edge structures correlate well with the different $d^n \rightarrow d^{n-1}$ multiplet structures, as predicted by conventional crystal-field theory and as seen in the low-energy ($\lesssim 3$ eV) or "main peak" portions of the valence-band photoemission spectra (*14, 32*). The observed absorption-edge structures therefore appear to be due to $3d \rightarrow 4s, 4p$ (band) transitions (*33, 34*). This assignment is also supported by modulation spectroscopies (electroreflectance and thermoreflectance) (*34*). It should be noted that the $3d$ designation here refers to an antibonding $3d$-$2p$ admixture, as in molecular-orbital theory, so its energy differs from that of the "bare" $3d$ basis state of the model.

We presume that the CuO electrical conductivity (photocurrent) gap reported (*35*) at 1.35 eV represents the optical absorption edge, and is also due to $3d \rightarrow 4s$, $4p$ (band) transitions. This was, effectively, the experimental assignment (*35*). This differs from the well-known assignment of Zaanen, Sawatzky, and Allen (*5*), namely $2p \rightarrow 3d$. Nevertheless, the present assignment has a long history in the field of transition metal oxides (*33, 34*), and at one time this was widely accepted. It should be noted that this threshold energy lies significantly below the Mott energy, for $d^n + d^n \rightarrow d^{n-1} + d^{n+1}$ transitions, denoted here by U_{Mott}. Our data analysis is based on U_{Mott} rather than the conductivity gap, in contrast to ETS, because U_{Mott} relates to the present model more directly and unambiguously.

Another motivation for the present study has been to explore the feasibility of a cuprate superconductivity pairing mechanism (*12*) based on the valence-fluctuation or heavy-fermion type of "normal state" above T_c. The present results do tend to support that scenario, since that mechanism requires a large value for Δ. In that picture, the present $^1A_1$ threshold photoemission state corresponds to the Kondo singlet state which results from Kondo screening of the usual copper d^9 local moment. The existence of a normal Fermi-liquid state above T_c is made possible by the elimination, in this manner, of all of the local moments (*36*). (The occurrence of a local $^1A_1$ state at each copper ion, rather than a d^9 local moment configuration, is such a radical difference that this valence-fluctuation phase should presumably be separated from the Mott-insulator phase of CuO or pure La_2CuO_4 by a first-order transition.)

On the other hand, much evidence against the present configuration-energy scheme was cited in the Introduction. We concluded there, however, that only the evidence from the resonant photoemission (*15*) requires a careful examination here. It is certainly true that much stronger resonance is observed in the satellite region than in or near the main peak. Following the standard treatment of the resonance phenomenon (*37*), this is interpreted as direct evidence for the d^8 spectral density being concentrated at high binding energy, thereby implying a high value for $E(d^8)$. We now offer a counterargument. This is

based on the strong evidence for adiabaticity at 70 eV, and therefore also at the $3p \rightarrow 3d$ resonance around 74 eV photon energy. This evidence (strong suppression of the satellite intensity) indicates that the departure of the photoelectron is slow enough to produce some adiabatic $2p \rightarrow 3d$ charge transfer, via increased covalency, in the direct (non-resonant) photoemission channel. It then follows that there should also be some corresponding charge transfer in the resonance channel, and therefore some $d^9\underline{L}$ component in the resonance final state. (The conventional resonance channel is $3d^9 + h\nu \rightarrow 3p^{-1}3d^{10} \rightarrow 3d^8 + \varepsilon_k$, which interferes with the direct photoemission.) With a suitable phase, this $d^9\underline{L}$ component could reduce the resonance strength for states near the main peak, and increase this for states in the satellite, so that this might reconcile the resonance data with the present energy scheme.

We now outline an argument that the resonance channel $d^9\underline{L}$ component does have this phase. We use a semiclassical treatment (*29*) of the time evolution of the satellite state (Ψ_{sat}) component amplitude, within the resonance channel wavefunction, while the photoelectron is departing. We assume that the total wavefunction for this channel can be described as a linear combination of the Ψ_{sat} and Ψ_{mp} (mp = main peak) states, and similarly for the direct photoemission channel. In this treatment, the driving term for the time evolution is $\langle \Psi_{sat} | \partial H/\partial t | \Psi_{mp} \rangle$. We visualize $\partial H/\partial t$ as the classical time-dependent Coulomb potential of the departing photoelectron, and we observe that this time derivative should be largest on the copper site. We also replace $\Psi^*_{sat}\Psi_{mp}$ by $\Psi_{AB}\Psi_B$, the product of antibonding and bonding combinations of the d and p orbitals of b_{1g} symmetry. The Ψ_{AB} and Ψ_B both evolve with time, via a time-dependent mixing angle, thereby describing the adiabatic $2p \rightarrow 3d$ charge transfer taking place within the particular channel wavefunction. We attribute the difference in the behaviors of the direct and resonance channels to their different signs for $\Psi_{AB}\Psi_B$ on the copper site at $t = 0$, since the direct-channel wavefunction commences with the ground-state ($d^9 + d^{10}\underline{L}$) mixing angle, while the resonance-channel wavefunction commences with $\theta = 0$, i.e., with a pure d^8 configuration. (It is essential to recall, here, that the present orbitals are really Wannier functions, which therefore have tails of opposite sign on the neighboring sites.) This difference leads to opposite signs for $\langle \Psi_{sat} | \partial H/\partial t | \Psi_{mp} \rangle$, for the wavefunctions of the direct and resonance channels, which causes their $d^9\underline{L}$-component mixing angles to evolve in opposite directions. This difference in the behavior of the mixing angles is, qualitatively, what is needed to resolve the apparent contradiction between the suppressed satellite intensity and the enhanced satellite resonance.

Another feature which deserves some comment is the discrepancy between the present finding of a very large Δ, and the considerably smaller Δ values (1.5–4 eV) obtained from sophisticated band-theoretic studies (*8, 9*). These band-theoretic studies are all based on the assumed validity of the local density approximation. We have shown elsewhere (*38*) that the breakdown of the local density approximation, for the Mott insulator materials (which include NiO, CuO, and La_2CuO_4), is due to its failure to properly distinguish between the five spatially distinct kinds of d orbitals. When U is sufficiently large, *the angle-dependent aspect of the nonlocal exchange potential* is able to produce an *orbital polarization* within individual Bloch functions, and thereby for the total wave function. This polarization (which is also spin dependent) is responsible for opening up (or else greatly increasing) the insulating gap, and likewise for the creation (or enhancement) of the local moments. Naively, one might expect

that the local-density value for ε_d would correspond to the average of the $d^8 \rightarrow d^9$ and $d^9 \rightarrow d^{10}$ addition energies (before hybridization), thus a proper treatment of U should increase Δ by roughly $\frac{1}{2}U$. This simple estimate does indeed account for the sign and general magnitude of the discrepancy.

Of course, all of our quantitative results are subject to the presumed validity of the Anderson impurity model. They may therefore change somewhat if the finite density and periodicity of the copper ions can somehow be taken into account. The present incorporation of copper 4*s* orbitals on a periodic lattice suggests a way that this might be accomplished. One can envisage having hybridizing 3*d* orbitals on each of the Pd sites of our tight-binding PdO lattice model, but with a reduced hybridization strength to take account, in a mean-field manner, of the inhibition to hybridization caused by the Hubbard U. An essential part of this program would then be to somehow remove the mean-field effect of the 3*d*'s on the selected "impurity" site, before proceeding with a detailed treatment of the present type for these "impurity" 3*d* orbitals. This scheme might then be iterated to self-consistency.

In any event, there is an indication that changes of order 10% in some of the parameters may be needed. This comes from the fact that the present parameters lead to a magnetic superexchange coupling J which is too small, compared to experiment, by about a factor of 2.

Conclusions

The previous analyses of photoemission and BIS data for CuO and other cuprates have presumed that essentially all of the desired information can be obtained from the 3*d*-removal spectrum alone. We have now demonstrated that additional information contained in the 2*p*-removal spectrum is vitally important for a reliable parameter determination. It is now clear that the nonhybridizing part of the 2*p* spectrum is particularly useful here, because (a) this is a major fraction of the total 2*p* intensity, (b) this can have distinctive and prominent features, and (c) it is obvious that the position of the latter, with respect to the 3*d*-removal features, is mainly determined by the parameter Δ. These considerations have led, quite unambiguously, to a major revision of the value of Δ, and an even larger change in the important difference $\Delta - U_{\text{eff}}(^1A_1)$. Inclusion of an additional parameter Δ_{CF}° was essential for this result, but this feature (a significant nonhybridization contribution to the crystal-field splitting) has been well established by ab initio cluster calculations. The other refinements we have employed likewise have independent justifications. On the other hand, the most persuasive evidence for the prevailing configuration-energy scheme, from resonant photoemission, was argued to be unreliable, due to an expected strong adiabatic correction to the sudden approximation. We believe that these conclusions should also apply, qualitatively, to a number of other transition-metal compounds, and in particular to NiO.

The present parameters should be much closer to the ones appropriate for Anderson lattice models of the superconducting cuprates, at least when Coulomb interactions involving the 2*p* electrons are neglected (*39*). In such an application, however, it is important to consider that Δ can be significantly affected by the Madelung potential effects of the ions between the CuO_2 layers, and especially by the presence or absence of apical oxygens (*40*).

Acknowledgments

I am indebted to many people for helpful discussions, correspondence, and unpublished material, especially

J. W. Allen, E. E. Alp, A. J. Arko, D. E. Eastman, D. R. Jennison, R. S. List, R. L. Martin, A. K. McMahan, M. A. Schluter, Z.-X. Shen, E. B. Stechel, J. B. Torrance, P. Weinberger, and J. Zaanen. I particularly want to thank G. A. Sawatzky for his helpful cooperation throughout this investigation. This work was supported by the U.S. Department of Energy. This paper is dedicated to Professor J. M. Honig, in appreciation for his fine work on transition-metal oxides.

References

1. S. Horn *et al., Phys. Rev. B* **36,** 3895 (1987); J. A. Yarmoff *et al., Phys. Rev. B* **36,** 3967 (1987); J. M. Tranquada *et al., Phys. Rev. B* **36,** 5263 (1987); N. Nücker *et al., Phys. Rev. B* **37,** 5158 (1988); A. Bianconi *et al., Int. J. Mod. Phys. B* **1,** 853 (1987); E. E. Alp, *et al., Phys. Rev. B* **40,** 9385 (1989).
2. A. Fujimori, E. Takayama-Muromachi, Y. Uchida, and B. Okai, *Phys. Rev. B* **35,** 8814 (1987); Z. Shen *et al., Phys. Rev. B* **36,** 8414 (1988); D. D. Sarma, *Phys. Rev. B* **37,** 7948 (1988); K. Okada and A. Kotani, *J. Phys. Soc. Japan* **58,** 1095 (1989); F. Mila, *Phys. Rev. B* **38,** 11,358 (1988); D. E. Ramaker, *Phys. Rev. B* **38,** 11816 (1988) (see also Ref. (*8*)).
3. J.Ghijsen *et al., Phys. Rev. B* **38,** 11,322 (1988).
4. H. Eskes and G. A. Sawatzky, *Phys. Rev. Lett.* **61,** 1415 (1988); H. Eskes, L. H. Tjeng, and G. A. Sawatzky, *in* "Mechanisms of High Temperature Superconductivity" (H. Kamimura and A. Oshiyama, Eds.), p. 20, Springer-Verlag, Heidelberg (1989); *Phys. Rev. B* **41,** 288 (1990).
5. G. A. Sawatzky and J. W. Allen, *Phys. Rev. Lett.* **53,** 2339 (1984); J. Zaanen, G. A. Sawatzky, and J.W. Allen, *Phys. Rev. Lett.* **55,** 418 (1985); J. Zaanen and G. A. Sawatzky, *Canad. J. Phys.* **65,** 1262 (1987).
6. G. van der Laan, C. Westra, C. Haas, and G. A. Sawatzky, *Phys. Rev. B* **23,** 4369 (1981); G. van der Laan, J. Zaanen, G. A. Sawatzky, R. Karnatak, and J.-M. Esteva, *Phys. Rev. B* **33,** 4253 (1986); J. Zaanen, C. Westra, and G. A. Sawatzky, *Phys. Rev. B* **33,** 8060 (1986).
7. J. Zaanen, Ph.D. thesis, University of Groningen (1986), unpublished.
8. A. K. McMahan, R. M. Martin, and S. Satpathy, *Phys. Rev. B* **38,** 6650 (1988).
9. M. S. Hybertsen, M. Schlüter, and N. E. Christensen, *Phys. Rev. B* **39,** 9028 (1989), and references therein.
10. E. E. Alp *et al., Phys, Rev. B* **35,** 7199 (1987); P. Steiner *et al., Z. Phys.B* **67,** 497 (1987), **66,** 275 (1987), and **69,** 449 (1988); W. Herzog *et al., Z. Phys. B* **71,** 19 (1988); B. Lengeler *et al., Solid State Commun.* **65,** 1545 (1988); M. Ospelt *et al., Physica C* **153–155,** 159 (1988). See also E. E. Alp *et al., J. Phys.: Condens. Matter* **1,** 6463 (1989).
11. R. S. List *et al., Phys. Rev. B* **38,** 11,966 (1988); *Physica C* **159,** 439 (1989); A. J. Arko and R. S. List, private communication.
12. B. H. Brandow, *Solid State Commun.* **69,** 915 (1989).
13. G. K. Wertheim and S. Hüffner, *Phys. Rev. Lett.* **28,** 1028 (1972).
14. D. E. Eastman and J. L. Freeouf, *Phys. Rev. Lett.* **34,** 395 (1975).
15. J. Ghijsen *et al.*, preprint; see also K. Okada and A. Kotani, Ref. (*2*).
16. A. Fujimori and F. Minami, *Phys. Rev. B* **30,** 957 (1984).
17. J. J. Yeh and I. Lindau, *At. Data Nucl. Data Tables* **32,** 1 (1985).
18. S. Åsbrink and L.-J. Norrby, *Acta Crystallogr., Sect. B* **26,** 8 (1970); W. J. Moore, Jr., and L. Pauling, *J. Amer. Chem. Soc.* **63,** 1392 (1941); J. Waser, H. A. Levy, and S. W. Peterson, *Acta Crystallogr.* **6,** 661 (1953).
19. L. F. Mattheiss, *Phys. Rev. B* **5,** 290 (1972).
20. J. C. Slater and G. F. Koster, *Phys. Rev.* **94,** 1498 (1954); W. A. Harrison, "Electronic Structure and the Properties of Solids," Freeman, San Francisco, (1980).
21. M. J. DeWeert, D. A. Papaconstantopoulos, and W. E. Pickett, *Phys. Rev. B* **39,** 4235 (1989); L. F. Mattheiss and D. R. Hamann, *Phys. Rev. B* **40,** 2217 (1989).
22. See, for example, McMahan *et al.*, Ref. (*8*).
23. A. Kotani *et al., Solid State Commun.* **53,** 805 (1985).
24. T. F. Soules, J. W. Richardson, and D. M. Vaught, *Phys. Rev. B* **3,** 2186 (1971); A. J. H. Wachters and W. C. Nieuwpoort, *Phys. Rev. B* **5,** 4291 (1972), and references therein.
25. Y. Tanabe and S. Sugano, *J. Phys. Soc. Japan* **9,** 766 (1954).
26. R. L. Martin and P. W. Saxe, *Int. J. Quantum Chem. Symp.* **22,** 2371 (1988); R. L. Martin, *Physica B,* **163,** 533 (1990), and private communication.
27. P. Ros and G. C. A. Schuit, *Theor. Chim. Acta (Berl.)* **4,** 1 (1966); B. Roos, *Acta Chem. Scand.* **20,** 1673 (1966); H. Basch and H. B. Gray, *Inorg. Chem.* **6,** 365 (1967); F. A. Cotton and C. B. Harris, *Inorg. Chem.* **6,** 369 (1967); J. Demu-

YNCK, A. VEILLARD, AND U. WAHLGREN, *J. Amer. Chem. Soc.* **95,** 5563 (1973).
28. B. H. BRANDOW, *Adv. Phys.* **26,** 651 (1977), Appendix E.
29. T. D. THOMAS, *Phys. Rev. Lett.* **52,** 417 (1984); *J. Electron Spectrosc.* **40,** 259 (1986). This work on atomic Ne suggests a far weaker effect than observed here, but we argue that the higher angular momentum of the 3*d* orbital (more tangential velocity, therefore less radial velocity) and the the larger relevant distance (the copper–oxygen separation) should considerably enhance the adiabaticity for the present case.
30. C. K. JØRGENSEN, "Absorption Spectra and Chemical Bonding in Complexes," Chap. 7, Pergamon, Oxford (1962); B. N. FIGGIS, "Introduction to Ligand Fields," Chaps. 5 and 9, Interscience, New York (1966).
31. P. W. ANDERSON, *Solid State Phys.* **14,** 99 (1963).
32. REF. (*28*), Sections 5.6.1 and 5.6.4.
33. R. J. POWELL AND W. E. SPICER, *Phys. Rev. B* **2,** 2182 (1970); D. Adler and J. Feinleib, *Phys. Rev. B* **2,** 3112 (1970).
34. L. MESSICK, W. C. WALKER, AND R. GLOSSER, *Phys. Rev. B* **6,** 3941 (1972); see also Ref. (*28*), p. 745.
35. F. P. KOFFYBERG AND F. A. BENKO, *J. Appl. Phys.* **53,** 1173 (1982).
36. There is a well-known objection to this picture by P. Nozieres [*Ann. Phys. (Paris)* **10,** 19 (1985)], who has argued that the available conduction electrons are insufficient to screen away all of the local moments. We have shown by explicit construction that this argument is invalid for the Anderson lattice model: B. H. Brandow, *Phys. Rev. B* **33,** 215 (1986), see p. 225.
37. L. C. DAVIS, *Phys. Rev. B* **25,** 2912 (1982), and references therein.
38. REF. (*28*), Sections 5.2, 5.3, 5.7.4, and Appendix D; B. H. Brandow, *in* "Narrow-Band Phenomená" (J. C. Fuggle, G. A. Sawatzky, and J. W. Allen, Eds.), p. 97, Plenum, New YorK (1988).
39. For Hamiltonians which include Coulomb interactions with 2*p* electrons, see Refs. (*3, 8* (appendix), and *9*), and E. B. Stechel and D. R. Jennison, *Phys. Rev. B* **38,** 4632 (1988).
40. J. B. TORRANCE AND R. M. METZGER, *Phys. Rev. Lett.* **63,** 1515 (1989).